Sensorless Full-Digital PMSM Drive With EKF Estimation of Speed and Rotor Position

Silverio Bolognani, Roberto Oboe, and Mauro Zigliotto

***Abstract*— This paper concerns the realization of a sensorless permanent magnet (PM) synchronous motor drive. Position and angular speed of the rotor are obtained through an extended Kalman filter. The estimation algorithm does not require either the knowledge of the mechanical parameters or the initial rotor position, overcoming two of the main drawbacks of other estimation techniques. The drive also incorporates a digital d–q current control, which can be easily tuned with locked rotor. The experimental setup includes a PM synchronous motor, a pulsewidth modulation voltage-source inverter, and floating-point digital-signal-processor-based control system.**

***Index Terms*— Kalman filtering, permanent magnet synchronous motor, sensorless drives.**

NOMENCLATURE

$\mathbf{B}$	Control matrix.
$\mathbf{f}(\mathbf{x})$	System state matrix.
$\mathbf{F}$	Partial derivative system matrix.
$\mathbf{H}$	Output matrix.
$\mathbf{K}$	Kalman filter gain matrix.
i	Stator current.
L_s	Synchronous inductance.
$\mathbf{P}$	State covariance matrix.
$\mathbf{Q}$	System noise covariance matrix.
$\mathbf{R}$	Measurement noise covariance matrix.
R_s	Stator resistance.
T_c	Sampling period.
$\mathbf{v}$	Stator phase voltage vector.
$\mathbf{x}, \mathbf{x}e$	Actual, estimated state vector.
$\mathbf{y}$	Output vector.
λ	Stator permanent magnet (PM) flux linkage.
μ	Measurement noise vector.
σ	System noise vector.
ϑ	Rotor position.
ω	Speed.

Subscripts and Superscripts

d, q	Two-axes synchronous frame quantities.
α, β	Two-axes stationary frame quantities.
k	Sampling index.
0	Initial value.
$k \mid k-1$	Predicted estimate.
$k \mid k$	Optimal estimate.
$'$	Transposed matrix.
$*$	Reference quantities.

Bold characters are used for vectors and matrices. The symbol $\langle \bullet k \rangle$ is used to indicate mean value in the interval from t_k to t_{k+1}.

Manuscript received May 20, 1997; revised June 2, 1998. Abstract published on the Internet October 26, 1998.

S. Bolognani and M. Zigliotto are with the Department of Electrical Engineering, University of Padova, 35131 Padova, Italy (e-mail: bolognan@dei.unipd.it.; mauroz@dei.unipd.it).

R. Oboe is with the Department of Electronics and Informatics, University of Padova, 35131 Padova, Italy (e-mail: oboe@dei.unipd.it).

Publisher Item Identifier S 0278-0046(99)00494-3.

II. INTRODUCTION

THE torque control of a permanent magnet synchronous motor (PMSM) drive needs the rotor position to perform an effective current control. Moreover, for a speed control, the speed signal is also needed. Synchronous motors used in ac drives are, therefore, usually equipped with an electromechanical sensor mounted on their shafts (resolver or absolute encoder).

Several methods have been developed in order to obtain rotor position and angular speed from the measurements of electric quantities, eliminating the need for sensors. The idea behind such methods is to manipulate the motor equations in order to express motor position and speed as functions of the terminal quantities. Most of the methods, however, work only with an anisotropic rotor and when the dependence of the inductance on the rotor position is accurately known; moreover, the speed is not estimated, thus the drive is not completely without mechanical sensors [1]–[3].

Other methods have been developed based on state observers, but linearization of the nonlinear equations describing the drive behavior along the nominal state trajectory does not guarantee the overall stability [4].

In [5] and [6], a model-based approach to sensorless control has been adopted. The results are smart and the implementation is quite effective, even if the sensitivity to the motor parameters could heavily affect the estimation, and the technique requires a preliminary rotor alignment. Last, the extension of the technique to anisotropic PMSM could be quite complicated, due to the increased complexity of the motor model.

Thanks to their ability to perform state estimation for nonlinear systems, extended Kalman filters (EKF's) have found wide application in the estimation of rotor position and speed in synchronous motor drives [7]–[16]. So far, however, computation requirements, parameter sensitivity, and initial conditions have unfavorably characterized this approach. In fact, only a few of the reported applications of EKF's to sensorless PMSM drives include closed-loop operations, and all of them require measurement and filtering of the applied voltage, accurate mechanical modeling, and known initial position.

As for the computational load, however, last-generation floating-point digital signal processors (DSP's) are now capable of tens of MFLOPS, and they can easily bear the EKF real-time calculations.

This paper describes the realization of a sensorless PMSM drive, in which a single floating-point DSP (WEDSP-32C from AT&T) performs the on-line calculations for the EKF, the current and speed control loops, and the space-vector pulsewidth modulation (SVPWM).

This paper follows and completes a previously published paper [16], where the theoretical aspects and some new features have been studied and successfully simulated. The main features are as follows.

1) The mechanical parameters are not required, and the problem of parameter sensitivity is partially overcome.
2) The measurement of the voltage applied to the motor is no longer required, ensuring an easier convergence of the EKF estimate. In fact, voltage measurements are affected by the modulation noise, so a filtering action is needed. This introduces a delay that could cause problems in the algorithm convergence. Since the inverter switching period is small with respect to the electrical time constant of the motor, it is possible to use the voltage references instead of the actual voltage, also taking into account the inverter saturation. A side effect is the further reduction of the sensor number, compared to other approaches.

This paper is organized as follows. The EKF algorithm and the nonlinear state-space model of the motor are first described. Then, the proposed drive structure is presented, as well as the speed and current control. After this, the experimental setup and results are described. The paper ends with some final considerations on the application.

III. The EKF Algorithm

The EKF is an optimal estimator in the least-square sense for estimating the states of dynamic nonlinear systems. For a straightforward application of this algorithm to the proposed drive, the motor nonlinear state equations are written in the following form:

$$\begin{aligned} \dot{\mathbf{x}}(t) &= \mathbf{f}[\mathbf{x}(t)] + \mathbf{B}\cdot\mathbf{v}(t) + \sigma(t); \\ \mathbf{y}(t_k) &= \mathbf{h}(\mathbf{x}(t_k)) + \mu(t_k) \end{aligned} \tag{1}$$

where $\sigma(t)$ and $\mu(t_k)$ are zero-mean white Gaussian noises with covariance $\mathbf{Q}(t)$ and $\mathbf{R}(t_k)$, respectively, and independent from the system state $\mathbf{x}$ and $t_k = kT_c$. The system noise $\sigma(t)$ takes into account the system disturbances and model inaccuracies, while $\mu(t_k)$ represents the measurement noise. The initial state vector $\mathbf{x}(t_0)$ is described as a Gaussian random vector with mean value $\mathbf{x}_0$ and covariance matrix $\mathbf{P}_0$, and $\mathbf{v}(t)$ is the deterministic input vector.

In order to get the system equations in the most suitable form, the motor has been described in a stationary two-axes reference frame (α, β). This choice yields to a model in which the derivative of the motor currents are linearly related to both currents and applied voltages. In addition, the dynamic model of the motor is derived under the so-called "infinite inertia" hypothesis. This means that the rotor speed derivative is considered negligible compared with the other system variables, and any mechanical load parameter, as well as the load torque, will disappear from the motor equations. By assuming

$$\mathbf{x} = [i_\alpha \quad i_\beta \quad \omega \quad \vartheta]', \quad \mathbf{v} = [v_\alpha \quad v_\beta]', \quad \mathbf{y} = [i_\alpha \quad i_\beta]' \tag{2}$$

the system matrices $\mathbf{f}(\mathbf{x})$, $\mathbf{B}$, and $\mathbf{h}(\mathbf{x})$ result [16]

$$\mathbf{f}(x) = \begin{bmatrix} f_1 \\ f_2 \\ f_3 \\ f_4 \end{bmatrix} = \begin{bmatrix} -\dfrac{R_s i_\alpha}{L_s} + \dfrac{\omega\lambda}{L_s}\cdot\sin\vartheta \\ -\dfrac{R_s i_\beta}{L_s} - \dfrac{\omega\lambda}{L_s}\cdot\cos\vartheta \\ 0 \\ \omega \end{bmatrix} \tag{3}$$

$$\mathbf{B} = \begin{bmatrix} \frac{1}{L_s} & 0 \\ 0 & \frac{1}{L_s} \\ 0 & 0 \\ 0 & 0 \end{bmatrix}, \quad \mathbf{h}(x) = \begin{bmatrix} i_\alpha \\ i_\beta \end{bmatrix}$$

where R_s and L_s are the motor phase resistance and synchronous inductance and λ is the PM flux linkage. For this system, which is clearly nonlinear, an EKF is derived. First of all, let us define the Jacobian matrices

$$\begin{aligned} \mathbf{F}(\mathbf{x}(t)) &= \left.\frac{\partial \mathbf{f}}{\partial \mathbf{x}}\right|_{\mathbf{x}=\mathbf{x}(t)} \\ &= \begin{bmatrix} -\dfrac{R_s}{L_s} & 0 & \dfrac{\lambda}{L_s}\sin\vartheta & \dfrac{\omega\lambda}{L_s}\cos\vartheta \\ 0 & -\dfrac{R_s}{L_s} & -\dfrac{\lambda}{L_s}\cos\vartheta & \dfrac{\omega\lambda}{L_s}\sin\vartheta \\ 0 & 0 & 0 & 0 \\ 0 & 0 & 1 & 0 \end{bmatrix} \\ \mathbf{H}(\mathbf{x}(t)) &= \left.\frac{\partial \mathbf{h}}{\partial \mathbf{x}}\right|_{\mathbf{x}=\mathbf{x}(t)} = \begin{bmatrix} 1 & 0 & 0 & 0 \\ 0 & 1 & 0 & 0 \end{bmatrix}. \end{aligned} \tag{4}$$

According to (3), there is a linear relation between states and outputs, then the linearization of the system (1) is

$$\delta\dot{\mathbf{x}}(t) = \mathbf{F}(\mathbf{x}(t))\delta\mathbf{x}(t) + \sigma(t) \tag{5}$$

$$\mathbf{y}(t) = \mathbf{H}\mathbf{x}(t) + \mu(t). \tag{6}$$

After discretization with constant period T_c, (5) becomes

$$\delta\mathbf{x}(t_k) = \Phi(t_k, t_{k-1}, \mathbf{x}(t_{k-1}))\delta\mathbf{x}(t_{k-1}) + \nu(t_{k-1}) \tag{7}$$

where Φ is the exponential matrix for the linear system (5). Since its on-line calculation is quite heavy, its approximation

$$\Phi(t_k, t_{k-1}, \mathbf{x}(t_{k-1})) \cong \mathbf{I} + \mathbf{F}T_c \tag{8}$$

is normally used instead. For the discrete system noise ν, it is related to the continuous one by

$$\nu(t_k) = \int_{t_k}^{t_{k+1}} \Phi(t_{k+1}, s, \mathbf{x}(s))\sigma(s)\, ds \tag{9}$$

then its covariance matrix $\mathbf{Q}_d$ results

$$\mathbf{Q}_d(t_k) = \int_{t_k}^{t_{k+1}} \Phi(t_{k+1}, s, \mathbf{x}(s))\mathbf{Q}(s)\Phi'(t_{k+1}, s, \mathbf{x}(s))\, ds. \tag{10}$$

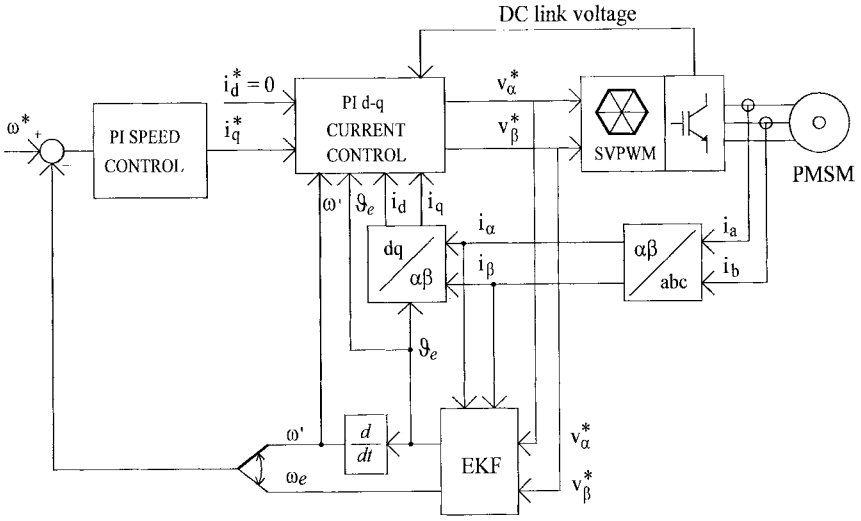

Fig. 1. The proposed sensorless drive.

Indeed, this covariance matrix is time varying, but its on-line calculation would be unbearable for a real-time implementation of the EKF. However, explicit calculation of (10) from a diagonal $\mathbf{Q}$ and (8) shows that $\mathbf{Q}_d$ is composed of a diagonal, time-invariant matrix, plus a time-varying matrix. The elements of the latter being at least two orders of magnitude smaller than the smallest element of the former, an acceptable approximation is to use a constant diagonal covariance matrix $\mathbf{Q}_d$ instead of (10). Moreover, given the above considerations, the EKF tuning can be performed directly on the value of $\mathbf{Q}_d$ elements [16]. Once the linearized and discretized version of (1) is obtained, it is easy to derive the EKF for the system.

For the given sampling time t_k, both the optimal state estimate sequence $\mathbf{xe}_{k|k}$ and its covariance matrix $\mathbf{P}_{k|k}$ are generated by the filter through a two-step loop.

The first one (prediction step) performs a prediction of both quantities based on the previous estimates $\mathbf{xe}_{k-1|k-1}$ and the mean voltage vector $\langle \mathbf{v}_{k-1} \rangle$ actually applied to the system in the period from t_{k-1} to t_k. In this paper, a simple rectangular integration technique is used, so that the aforementioned prediction step results in the following recursive equations:

$$\begin{aligned} \mathbf{xe}_{k|k-1} &= \mathbf{xe}_{k-1|k-1} + [\mathbf{f}(\mathbf{xe}_{k-1|k-1}) + \mathbf{B}\langle \mathbf{v}_{k-1} \rangle] T_c \\ \mathbf{P}_{k|k-1} &= \mathbf{P}_{k-1|k-1} + (\mathbf{F}_{k-1}\mathbf{P}_{k-1|k-1} \\ &\quad + \mathbf{P}_{k-1|k-1}\mathbf{F}'_{k-1}) T_c + \mathbf{Q}_d \end{aligned} \tag{11}$$

with $\mathbf{F}_{k-1}$ defined by (4), computed for $\mathbf{x} = \mathbf{xe}_{k-1|k-1}$.

The second step (innovation step) corrects the predicted state estimate and its covariance matrix through a feedback correction scheme that makes use of the actual measured quantities; this is realized by the following recursive relations:

$$\begin{aligned} \mathbf{xe}_{k|k} &= \mathbf{xe}_{k|k-1} + \mathbf{K}_k(\mathbf{y}_k - \mathbf{H}\mathbf{xe}_{k|k-1}) \\ \mathbf{P}_{k|k} &= \mathbf{P}_{k|k-1} - \mathbf{K}_k\mathbf{H}\mathbf{P}_{k|k-1} \end{aligned} \tag{12}$$

where the filter gain matrix $\mathbf{K}_k$ is defined by

$$\mathbf{K}_k = \mathbf{P}_{k|k-1}\mathbf{H}'(\mathbf{H}\mathbf{P}_{k|k-1}\mathbf{H}' + \mathbf{R})^{-1}. \tag{13}$$

For the on-line application of the Kalman filter, time constraints are critical; since most of the matrices contain a lot of null elements, all the calculations have been made explicit, saving computational time.

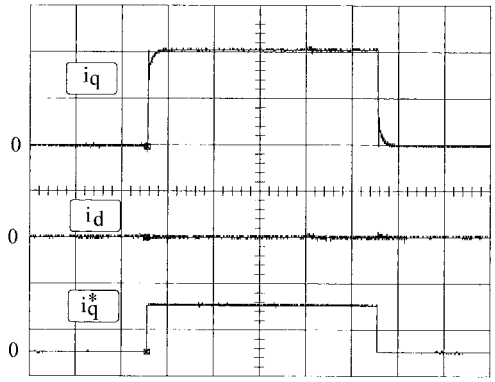

Fig. 2. Quadrature current loop step response, with locked rotor. x axis: 50 ms/div; y axes: 1 A/div (i_d, i_q), 2 A/div (i_q^*).

A quite open subject is the choice of the initial values for the matrices $\mathbf{R}$, $\mathbf{Q}_d$, and $\mathbf{P}_0$ that, in this paper, have been chosen with a trial-and-error procedure to get the best tradeoff between filter stability and convergence time [9]. Such matrices are reported as

$$\begin{aligned} \mathbf{Q}_d &= \begin{bmatrix} 0.4 & 0 & 0 & 0 \\ 0 & 0.4 & 0 & 0 \\ 0 & 0 & 16 & 0 \\ 0 & 0 & 0 & 2 \end{bmatrix}, \quad \mathbf{R} = \begin{bmatrix} 0.5 & 0 \\ 0 & 0.5 \end{bmatrix} \\ \mathbf{P}_0 &= \begin{bmatrix} 0.1 & 0 & 0 & 0 \\ 0 & 0.1 & 0 & 0 \\ 0 & 0 & 200 & 0 \\ 0 & 0 & 0 & 10 \end{bmatrix}. \end{aligned} \tag{14}$$

It has been stressed that $\mathbf{P}_0$ is by far the less influent choice in the initial tuning procedure of the Kalman filter.

Since the algorithm does not require the initial rotor position, and the motor is supposed to start from the standstill condition, the initial state vector $\mathbf{x}_0$ has been considered the null vector.

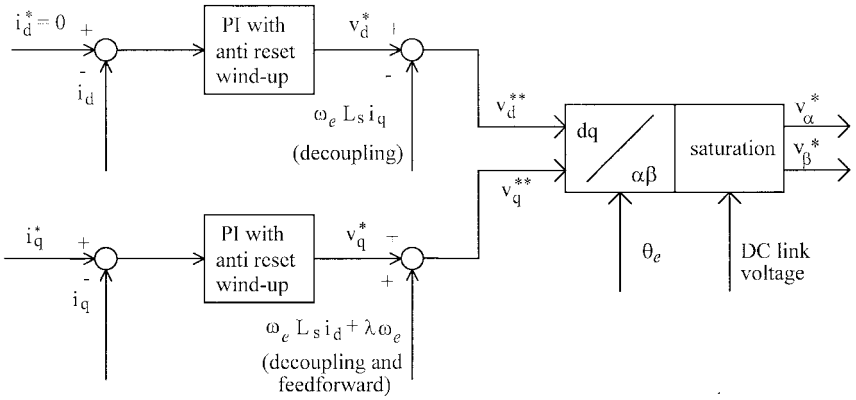

Fig. 3. d–q current control and voltage reference limitations.

IV. The Proposed Drive

A schematic of the proposed sensorless speed control of a PMSM is shown in Fig. 1; the complete drive also includes the power stage, consisting of an isotropic PMSM with sinusoidal EMF's fed by an insulated gate bipolar transistor (IGBT) voltage inverter. As depicted in Fig. 1, the proportional integral (PI) speed regulator compares the reference ω^* with the speed ω', calculated as a time derivative of the estimated position ϑ_e, or with the estimated speed ω_e, and it delivers as output the quadrature current reference i_q^*. A discussion of the drive performance with the two different speed feedback signals is reported later in this paper.

The direct current reference i_d^* is set equal to zero, to obtain the maximum torque-to-current ratio. The current control is realized first by decoupling the dynamics between the applied voltages and the currents according to the two axes d, q of the synchronous frame; this greatly simplifies the design of the current regulators [17]. A feedforward action, that takes into account the motor EMF's, is also added to speed up the control itself. Two conventional PI regulators have been implemented for the direct and quadrature components of the stator currents, the gains of which have been tuned on the real system, starting from those obtained through simulations based on a model of the whole system.

A comparison with a predictive current control [16] has highlighted quite similar performance. The increase of the computation time, experimented with the PI controllers, is compensated by a simpler tuning procedure and a reduced sensitivity to the possible electrical parameters mismatch. Fig. 2 shows the time response to a step reference of the quadrature component i_q^* with locked rotor; the current loop bandwidth is about 1 kHz.

The reference voltages for the SVPWM algorithm, v_α^* and v_β^*, referred to the two-axes stationary frame (α, β), are then obtained from the output v_d^* and v_q^* of the PI current regulators using the EKF rotor position estimate ϑ_e for the synchronous-to-stationary coordinate transformation.

It results from Fig. 1 that the EKF is fed with the reference voltages instead of the measured ones; this choice further reduces the number of sensors and A/D converters of the drive. On the other hand, saturation due to the limited dc-link voltage would result in differences between reference and actually applied voltages that would cause a wrong behavior of the EKF. Then, saturation phenomena have been taken into account in the current controller implementation, in order to limit the voltage references within the drive capabilities, as reported in Fig. 3.

The saturation levels of the current regulators are chosen in order to avoid saturation of the SVPWM algorithm; therefore, the required voltage vector is forced to remain within the circle that, in the complex plane, is inscribed in the hexagonal boundary relative to the six state vectors of the voltage inverter. Indeed, this solution does not fully exploit the inverter capabilities [19], but it greatly simplifies the software handling of saturation effects. The use of some overmodulation techniques [20] would enlarge the linear range of the SVPWM, but the related improvements in the current regulator loops have not been considered of peculiar importance in this paper.

V. Sensorless Drive Implementation

The proposed EKF algorithm has been implemented as a full-digital control system, that also incorporates the SVPWM algorithm and the current control, as shown in Fig. 1.

The EKF algorithm, as well as the speed and current controllers, have been implemented on a floating-point DSP system, based on WEDSP-32C, designed and prototyped at the University of Padova, Padova, Italy [18]. The system is capable of a peak performance of 25 MFLOPS and hosts all the peripherals, which can be configured by the user according to the experiment needs. In this case, the system features a 12-bit A/D module for current acquisition and a digital interface for data exchange with the SVPWM board.

As reported in the flow chart of Fig. 4, after initialization, the program waits for a real-time clock that synchronizes all the algorithm operations. In particular, the phase current acquisitions, performed by the DSP system through its A/D channels, have been synchronized with the beginning of the PWM period, and this precaution greatly reduces the measurement noise due to the modulation ripple.

After the current acquisition, the innovation step of the EKF is performed. Given the estimate in t_{k-1}, the EKF algorithm then predicts the state in t_k, with the sampling period T_c fixed to 200 μs, that corresponds to a switching frequency of 5 kHz.

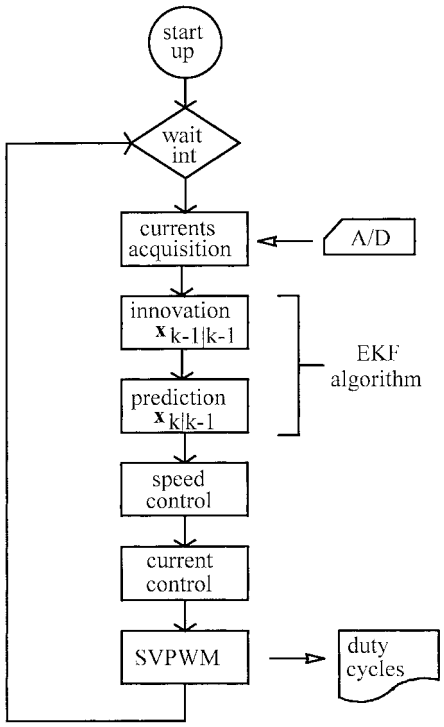

Fig. 4. Program flow chart.

TABLE I
COMPUTATION TIME

Current acquisition	15 μs
EKF algorithm	78 μs
Speed and current control	22 μs
SVPWM	28 μs
Total execution time	143 μs

As reported in Table I, the complete algorithm is executed in only 143 μs, but it can be easily reduced since, actually, many diagnostic analog signals are generated in run time. A set of simulations have indicated that an improvement in the convergence capability of the EKF could be derived, increasing the sampling rate up to 10 kHz.

VI. EXPERIMENTAL RESULTS

All the experimental results are obtained when current and speed loops operate using estimated speed and position. Either the estimated currents or the measured quantities (as suggested by the practice) have been used as current feedback with slight differences shown by the two solutions.

In the following figures, the measurements of the actual rotor speed and position have been obtained with the motor built-in resolver, using the Analog Devices 2S83 Resolver-to-Digital converter, that also provides an analog speed output. In Fig. 5, the measured rotor position is compared with the estimated one at constant speed. As a result, the estimated position shows good linearity and an almost perfect correspondence to the actual rotor position.

Fig. 6 reports the speed step response of the system with a PI speed controller with antireset windup feature. As it appears from the experiments, the speed loop has a bandwidth of about

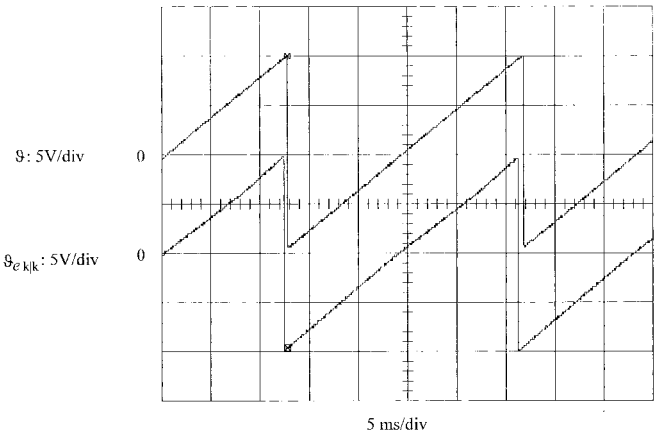

Fig. 5. Measured and estimated rotor position.

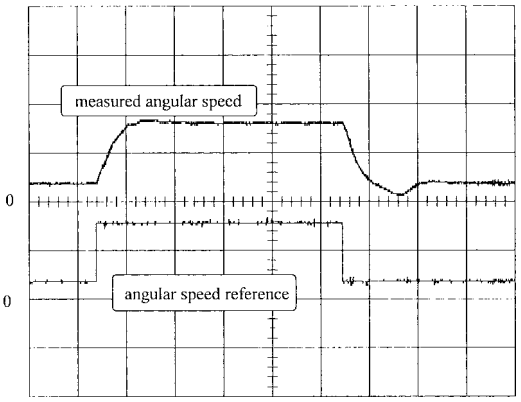

Fig. 6. Speed step response of the sensorless drive. x axis: 0.1 s/div; y axis: 40 rad/s/div.

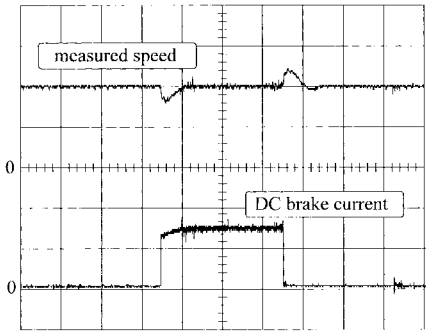

Fig. 7. Speed response to a step load torque variation. x axis: 0.2 s/div; y axes: 50 rad/s/div (speed), 5 A/div (current).

10 Hz. The speed loop has been closed on the derivative of the estimated position, since the experiments have shown that this signal is more reliable than the estimated speed itself. The latter may be, in fact, affected by a steady-state error mainly due to the aforementioned "infinite inertia" hypothesis. Such an error cannot be present in the derivative of the estimated position, provided that the current control is synchronized with the rotor position.

The last experimental result concerns the speed response to a step variation of the load torque, as reported in Fig. 7.

In the experimental setup, the load torque has been produced by a current-controlled dc motor coupled to the PMSM shaft

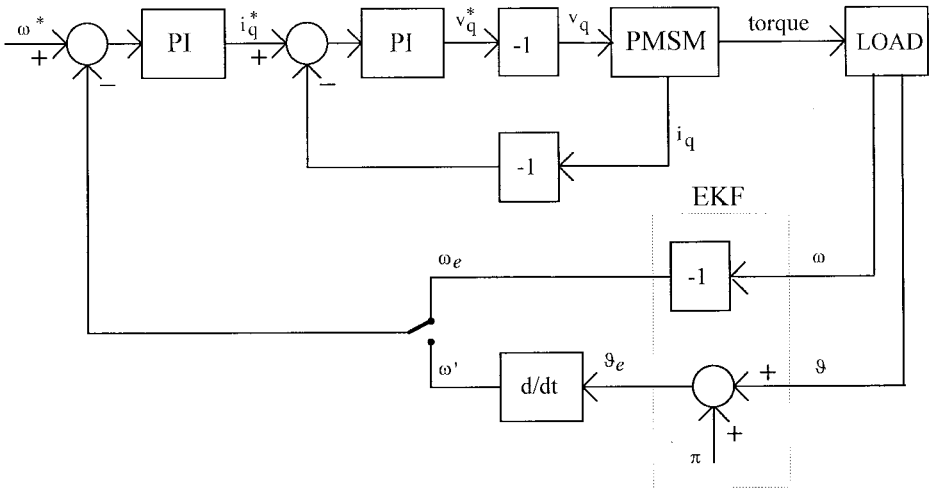

Fig. 8. Simplified schematic of the sensorless drive on wrong EKF convergence.

by a stiff joint. This system, of course, suffers from a limitation due to the finite bandwidth of the closed-loop control of the dc motor current. The lower part of Fig. 7 reports the behavior of the dc motor armature current, which is imposed to have a step variation of 7 A; since the torque constant of the adopted dc motor is 0.2 N·m/A, a corresponding torque of 1.4 N·m is generated, i.e., 50% of the PMSM rated one (see the Appendix).

A set of measurements has indicated that the drive operates quite appropriately down to 40 rad/s, that is, about 10% of the nominal speed; however, it suffers from some limitations regarding the torque delivery capability, in particular, at low speed. It has been found that the drive is negatively affected by the inverter deadtimes, which makes the actual motor voltages different from their references used by the EKF. However, deadtime effects can be easily compensated using, for example, the technique presented in [22]; the algorithm has already been tested by the authors in other drive applications, but it has not been included here because of the limited resources of the processor used in the experiments. On the contrary, inaccuracy in the current feedback due to sensor errors has been accurately avoided, by a precise gain calibration and an automatic offset compensation algorithm.

Corruption of the feedback signal due to the fast IGBT dynamic and the power cables [21] may also affect the current measurements, partially invalidating the usual zero-mean Gaussian noise statistical description adopted in (1). The analytical approach to the EKF convergence in the presence of a more complex noise statistical description could be quite involved; however, simulation and experimental tests have proved that the influence of a small nonzero mean noise in the measurements has the only side effect of a limited steady-state error in the estimated state.

Extremely long power cables and/or EMI polluted environment causes convergence problems for the EKF; EMI effects need to be reduced through an accurate hardware layout that comprises multilayer PCB's, switch snubbers, and EMI filtering, while the high-frequency currents due to the cable parasitic parameters can be mitigated by lengthening the rise time of the power switches.

VII. Effects and Countermeasures of Wrong Convergence at the Startup

It can be recognized that the motor voltage equations, referred to the (α, β) stationary frame, admit two acceptable solutions, that is, the correct solution (ω, ϑ) and a wrong one $(-\omega, \vartheta + \pi)$. Obviously, the wrong solution does not fit the state equation $\omega = d\vartheta/dt$; nevertheless, the EKF estimates can converge to it, since the innovation step always remedies for the wrong position predicted value. This works if $Q(4,4)$ is sufficiently high, while small or null values of $Q(4,4)$ avoid the wrong convergence, but make the convergence itself extremely slow [16].

Wrong convergence effects on the drive behavior, adopting the two different speed feedback signals mentioned above, can be studied in Fig. 8. In the figure, only the speed and quadrature current loops are shown, but the following discussion can be enlarged to the direct current loop, also. Under correct convergence, and neglecting steady-state errors and filter dynamics, the EKF behaves as an ideal speed and position transducer, as shown in Fig. 8.

In the case of wrong convergence, the dashed blocks represented in Fig. 8 appear, affecting the overall performance, as discussed in the following.

1) The position error of π does not affect the speed ω', which remains always coincident with the actual speed.
2) The effects of the position error on the $dq/\alpha\beta$ and $\alpha\beta/dq$ transformations have been represented in Fig. 8 by two unity negative gains, placed in both the direct and feedback paths of the current loop. The current loop dynamic is, hence, not affected, but the motor quadrature current is opposite its reference. This is equivalent to placing a unity negative gain in the direct path of the speed loop. If the speed feedback ω' is used, the closed loop becomes, of course, unstable. The output of the

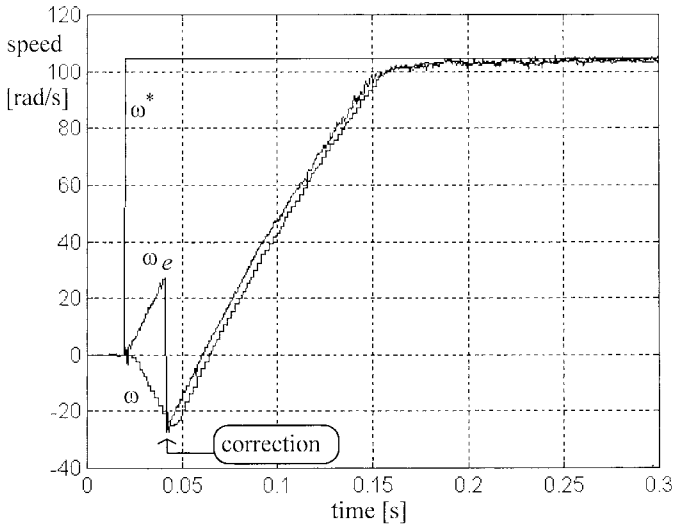

Fig. 9. EKF wrong convergence and correction action.

speed controller saturates to its maximum value and the drive operates in torque control mode with the speed limited by the available voltage or by the load torque. If the signal ω_e is used, a further unity negative gain is inserted in the loop, the system remains stable, but the speed becomes opposite its reference [16].

3) It is easy to realize that the conclusions reported above apply also for stationary current controllers, such as, for example, the predictive ones.

In this paper, a simple software countermeasure has been implemented against the wrong convergence. It intervenes only after the EKF convergence, for example, when the $\mathbf{P}(4,4)$ element becomes sufficiently small. Let us consider the time interval from t_{k-1} to t_k; the wrong convergence is recognized by the condition

$$\omega_{e_{k|k-1}} \cdot (\vartheta_{e_{k|k-1}} - \vartheta_{e_{k-1|k-2}}) < 0 \tag{15}$$

which states the opposite sign of ω_e and ω'.

If (15) holds, the routine simply states that

$$\omega_{e_{k|k-1}} = -\omega_{e_{k|k-1}}, \qquad \vartheta_{e_{k|k-1}} = \vartheta_{e_{k|k-1}} - \pi. \tag{16}$$

Several simulations and experimental tests have pointed out that the phenomenon of the wrong convergence appears only when the assumed initial value $\mathbf{x}_0$ differs by more than $\pi/2$ electrical rads from the actual one; the control statements (15) and (16) nullify the gap between actual and estimated position. Experimental evidence about the wrong convergence recognition and the consequent remedial action is reported in Fig. 9.

VIII. Conclusion

This paper has described the realization of a DSP-based estimation of speed and rotor position of a PM synchronous motor, using an EKF. The careful implementation has led to both reduction of computational time and extreme reduction of sensors, limited to the current and dc-link voltage transducers. The drive operates quite appropriately down to 40 rad/s, that is, about 10% of the nominal speed, even if the negative effects of the inverter deadtimes and the electromagnetic switching noise cause some limitations on the torque capability, in particular, at low speed. However, the experimental results are in good agreement with the expectation, and their employment in a high-performance drive is planned for the future.

Appendix
Motor Parameters

The technical data for the motor used in the experimental setup are as follows:

continuous duty nominal torque	2.8 N·m;
base speed	419 rad/s;
pole number	8;
stator resistance	1.9 Ω;
synchronous inductance	3 mH;
flux linkage	0.1 V·s;
rotor inertia	0.000 18 N·m·s^2.

Acknowledgment

The authors wish to thank Prof. D. Ciscato for his helpful suggestions and RVM srl, Torino, Italy, for providing the PMSM.

References

[1] H. Watanabe, T. Isii, and T. Fujii, "DC-brushless servo-system without rotor position and speed sensor," in *Proc. IEEE-IECON'87*, 1987, pp. 228–234.
[2] A. B. Kulkarni and M. Ehsani, "A novel position sensor elimination technique for the interior permanent-magnet synchronous motor drive," in *Conf. Rec. IEEE-IAS Annu. Meeting*, 1989, pp. 773–779.
[3] K. J. Binns, D. W. Shimmin, and K. M. Al-Aubidy, "Implicit rotor position sensing for permanent magnet self-commutating machine-drives," in *Proc. Int. Conf. Electrical Machines*, 1990, pp. 1231–1236.
[4] L. A. Jones and J. H. Lang, "A state observer for permanent-magnet synchronous motor," *IEEE Trans. Ind. Electron.*, vol. 36, pp. 374–382, June 1989.
[5] N. Matsui, "Sensorless operation of brushless DC motor drives," in *Proc. IEEE IECON'93*, 1993, pp. 739–744.
[6] N. Matsui and M. Shigyo, "Brushless DC motor control without position and speed sensors," in *Conf. Rec. IEEE-IAS Annu. Meeting*, 1990, pp. 448–454.
[7] A. M. N. Lima, B. de Fornel, and Mrs. Pietrzak-David, "On stochastic filtering technique and its applications to AC numerical drive systems," in *Proc. European Power Electronics Conf.*, 1987, pp. 683–688.
[8] P. K. Sattler and K. Stärker, "Control of an inverter fed synchronous machine by estimated pole position," in *Proc. IEEE PESC'88*, 1988, pp. 415–422.
[9] H.-G. Yeh, "Real-time implementation of a narrow-band Kalman filter with a floating-point processor DSP32," *IEEE Trans. Ind. Electron.*, vol. 37, pp. 13–18, Feb. 1990.
[10] P. K. Sattler and K. Stärker, "Estimation of speed and pole position of an inverter fed permanent excited synchronous machine," in *Proc. European Power Electronics Conf.*, 1989, pp. 1207–1212.
[11] S. Liu and M. Stiebler, "State estimation of a PWM inverter fed synchronous motor by using stochastic filtering techniques," in *Proc. Int. Conf. Electrical Machines*, 1990, pp. 1206–1211.
[12] R. Dhaouadi and N. Mohan, "Application of stochastic filtering to a permanent magnet synchronous motor-drive system without electro-mechanical sensors," in *Proc. Int. Conf. Electrical Machines*, 1990, pp. 1225–1230.
[13] M. Schroedl, "Control of a permanent magnet synchronous machine using a new position-estimator," in *Proc. Int. Conf. Electrical Machines*, 1990, pp. 1218–1224.
[14] R. Dhaouadi and N. Mohan, "DSP-based control of a permanent magnet synchronous motor with estimated speed and rotor position," in *Proc. European Power Electronics Conf.*, 1991, pp. 596–602.

[15] R. Dhaouadi, N. Mohan, and L. Norum, "Design and implementation of an extended Kalman filter for the state estimation of a permanent magnet synchronous motor," *IEEE Trans. Power Electron.*, vol. 6, pp. 491–497, July 1991.
[16] A. Bado, S. Bolognani, and M. Zigliotto, "Effective estimation of speed and rotor position of a PM synchronous motor drive by a Kalman filtering technique," in *Proc. IEEE PESC'92*, 1992, pp. 951–957.
[17] P. Vas, *Vector Control of AC Machines*. Oxford, U.K.: Clarendon, 1990.
[18] D. Ciscato and R. Oboe, "High performance robot controller based on WEDSP-32C," in *Proc. Workshop on Motion Control for Intelligent Automation*, 1992, pp. 120–125.
[19] J. Holtz, "Pulsewidth modulation—A survey," *IEEE Trans. Ind. Electron.*, vol. 39, pp. 410–420, 1992.
[20] S. Bolognani and M. Zigliotto, "Novel digital continuous control of SVM inverters in the overmodulation range," in *Proc. IEEE APEC'96*, 1996, pp. 219–223.
[21] R. J. Kerkman, D. Leggate, and G. Skibinski, "Interaction of drive modulation and cable parameters on AC motor transients," *IEEE Trans. Ind. Applicat.*, vol. 33, pp. 722–731, May/June 1997.
[22] J. W. Choi and S. K. Sul, "Inverter output voltage synthesis using novel dead-time compensation," *IEEE Trans. Ind. Electron.*, vol. 11, pp. 221–227, Apr. 1996.

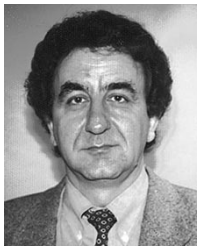

Silverio Bolognani was born in Trento Province, Italy. He received the laurea degree in electrical engineering from the University of Padova, Padova, Italy, in 1976.

In 1976, he joined the Department of Electrical Engineering, University of Padova, where he was involved in the analysis and design of thyristor converters and synchronous motor drives. He later founded the Electrical Drives Laboratory and conducted research on brushless and induction motor drives. He is presently engaged in research on advanced control techniques for motor drives and motion control and the design of ac electrical motors for variable-speed applications. He is the author of more than 80 technical papers on electrical machines and drives. His teaching activity was first devoted to electrical circuit and electromagnetic field theory and, later, to electrical drives and electrical machine design. He is currently an Associate Professor of Electrical Drives.

Roberto Oboe was born in Lonigo, Italy, in 1963. He recieved the degree and the doctoral degree in industrial electronics and computer science from the University of Padova, Padova, Italy, in 1988 and 1992, respectively.

Since 1993, he has been an Assistant Professor in Automatic Control in the Department of Electronics and Informatics, University of Padova. His current research is focused on applied digital control, telerobotics, virtual mechanisms, and Internet-based control.

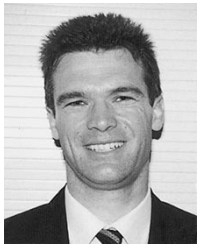

Mauro Zigliotto was born in Vicenza, Italy, in 1963. He received the degree in electronic engineering from the University of Padova, Padova, Italy, in 1988.

He originally worked in industry, dealing with the design and development of microcontroller-based circuits for industrial drives. In 1991, he joined the Electrical Drives Laboratory, Department of Electrical Engineering, University of Padova. Since 1995, he has been an Assistant Professor of Electrical Drives. His current research interests are in the area of innovative control strategies and their applications to motion control.